

# Basal and thermal control mechanisms of the Ragnhild glaciers, East Antarctica

Frank PATTYN, Sang DE BRABANDER, Ann HUYGHE

*Department of Geography, Vrije Universiteit Brussel, Pleinlaan 2, B-1050 Brussels, Belgium  
E-mail: fpattyn@vub.ac.be*

**ABSTRACT.** The Ragnhild glaciers are three enhanced-flow features situated between the Sør Rondane and Yamato Mountains in eastern Dronning Maud Land, Antarctica. We investigate the glaciological mechanisms controlling their existence and behavior, using a three-dimensional numerical thermo-mechanical ice-sheet model including higher-order stress gradients. This model is further extended with a steady-state model of subglacial water flow, based on the hydraulic potential gradient. Both static and dynamic simulations are capable of reproducing the enhanced ice-flow features. Although basal topography is responsible for the existence of the flow pattern, thermomechanical effects and basal sliding seem to locally soften and lubricate the ice in the main trunks. Lateral drag is a contributing factor in balancing the driving stress, as shear margins can be traced over a distance of hundreds of kilometers along west Ragnhild glacier. Different basal sliding scenarios show that central Ragnhild glacier stagnates as west Ragnhild glacier accelerates and progressively drains the whole catchment area by ice and water piracy.

## INTRODUCTION

The East Antarctic ice sheet is traditionally considered a stable feature characterized by slow-moving interior ice with drainage through ice shelves across a grounding line and by a few faster-moving outlet glaciers. This view is now challenged by new evidence coming from balance velocities (the depth-averaged velocity required to keep the ice sheet in steady state for a given net surface mass accumulation) obtained from radar altimetry and radio-echo sounding, as well as surface velocities obtained from interferometric synthetic aperture radar (Bamber and others, 2000). Complex ice flow (a combination of ice flow due to internal deformation and basal motion) was already observed within the West Antarctic and Greenland ice sheets (Joughin and others, 1999, 2001), and recent studies confirm a similar complexity within the East Antarctic ice mass (Pattyn and Naruse, 2003; Rippin and others, 2003). Balance-velocity maps reveal a complex network of enhanced-flow tributaries penetrating several hundred kilometers into the ice-sheet interior (Bamber and others, 2000; Testut and others, 2003). In this paper, we investigate such features observed in Dronning Maud Land, East Antarctica, and try to disentangle the mechanisms that control their existence and behavior with a three-dimensional thermomechanically coupled ice-sheet model including higher-order stress gradients, coupled to a steady-state model of basal water flow.

## DATA

The Ragnhild glaciers are three, as yet nameless, ice-flow features situated between the Sør Rondane and Yamato Mountains in eastern Dronning Maud Land. They are clearly identified as enhanced ice-flow features in maps of balance fluxes of the Antarctic ice sheet. The largest feature, here referred to as west Ragnhild glacier (WRG), penetrates almost 400 km inland (Fig. 1). RADARSAT imagery reveals distinct flowlines along the ice surface, but they are less apparent than those of other large ice streams and outlet glaciers of East Antarctica. A comparison between 1937

Norwegian maps and 1960 Belgian maps permitted (Nishio and others, 1984) determination of the horizontal movement of the ice-shelf front along the Princess Ragnhild Coast. Derwael Ice Rise is situated directly in front of WRG, so most of the ice flow is diverted around this buttressing feature. The maximum flow speed occurs at the western side ( $350 \text{ m a}^{-1}$ ), while flow velocities to the east of Derwael Ice Rise are somewhat lower. A comparison between 1965 Belgian maps and RADARSAT imagery (Jezek and RAMP Product Team, 2002) shows an acceleration in the west and a deceleration towards the east along the Princess Ragnhild Coast (Table 1). The latter might indicate an eventual stoppage of the glaciers in the center and the east of the catchment area. Ice-flow measurements in the interior of the drainage basin are sparser, but clearly mark a velocity of  $100 \text{ m a}^{-1}$  on WRG between the Sør Rondane and Belgica Mountains (Takahashi and others, 2003). This is relatively fast for typical ice-sheet flow so far inland. According to Bindschadler and others (2001),  $100 \text{ m a}^{-1}$  can be considered the lower limit of ice-stream flow in Antarctica. Ice speed on central Ragnhild glacier (CRG) is distinctly lower.

If these stream features exist, they are to a certain extent topographically controlled. Airborne radar surveys reveal that the coastal mountain blocks are interspersed by large subglacial valleys with their floors lying below sea level (Nishio and others, 1995). These ice-thickness measurements, included in the BEDMAP database (Liu and others, 1999; Lythe and others, 2001), form the major source material for the numerical experiments carried out below. For the prognostic experiments, surface mass balance was taken from Vaughan and others (1999).

## MODEL DESCRIPTION

The model approach is based on continuum thermodynamic modelling, and encompasses balance laws of mass, momentum and energy, extended with a constitutive equation. A complete description of the model is given in Pattyn

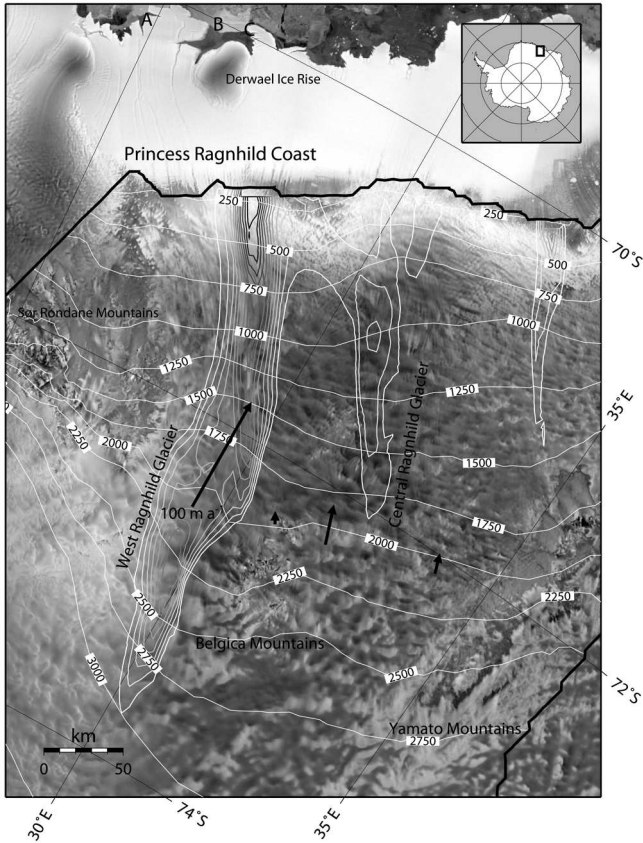


**Fig. 1.** Satellite image map based on RADARSAT-RAMP (RADAR-SAT-1 Antarctic Mapping Project) imagery (Jezek and RAMP Product Team, 2002). The thick black line delimits the modeled drainage basin (only part of the catchment is shown). Measured velocities (arrows) are taken from Takahashi and others (2003). Calculated balance fluxes are shown in gray-shaded contours (unlabeled); surface topography (m a.s.l.) in white contours.

(2003). The force-balance equations are

$$\frac{\partial}{\partial x} (2\sigma'_{xx} + \sigma'_{yy}) + \frac{\partial \sigma_{xy}}{\partial y} + \frac{\partial \sigma_{xz}}{\partial z} = \rho_i g \frac{\partial z_s}{\partial x}, \quad (1)$$

$$\frac{\partial}{\partial y} (2\sigma'_{yy} + \sigma'_{xx}) + \frac{\partial \sigma_{xy}}{\partial x} + \frac{\partial \sigma_{yz}}{\partial z} = \rho_i g \frac{\partial z_s}{\partial y}, \quad (2)$$

where  $\sigma_{ij}$  are the shear stress and  $\sigma'_{ii}$  the deviatoric normal stress components,  $\rho_i$  is the ice density,  $g$  is the gravitational constant and  $z_s$  is the surface elevation of the ice mass. The constitutive equation governing the creep of polycrystalline ice and relating the deviatoric stresses to the strain rates, is taken as a Glen-type flow law with exponent  $n = 3$  (Paterson, 1994):

$$\sigma'_{ij} = 2\eta \dot{\epsilon}_{ij}, \quad \eta = \frac{1}{2} A (\theta^*)^{-1/n} \dot{\epsilon}^{(1-n)/n}, \quad (3)$$

where  $\dot{\epsilon}$  is the second invariant of the strain-rate tensor and  $\eta$  is the effective viscosity. The flow-law rate factor is a function of temperature  $\theta$  ( $\theta^*$  is the temperature corrected for the dependence on pressure melting) and obeys an Arrhenius relationship. The temperature distribution reflects conduction, horizontal and vertical advection, and internal friction due to deformational heating:

$$\rho_i c_p \frac{\partial \theta}{\partial t} = k_i \frac{\partial^2 \theta}{\partial z^2} - \rho_i c_p \left( v_x \frac{\partial \theta}{\partial x} + v_y \frac{\partial \theta}{\partial y} + v_z \frac{\partial \theta}{\partial z} \right) + 2\dot{\epsilon} \sigma, \quad (4)$$

**Table 1.** Velocity estimates ( $\text{m a}^{-1}$ ) of the ice shelf along the Princess Ragnhild Coast, 1937–60 (Nishio and others, 1984), and 1965–97 (this study). Markers correspond to positions in Figure 1

Marker	1937–60	1965–97
A	350	382
B	300	218
C	205	127

where  $c_p$  and  $k_i$  are heat capacity and thermal conductivity of the ice, respectively,  $v_i$  are the velocity components, and  $\sigma$  is the second invariant of the stress tensor.

Instead of modelling the whole Antarctic ice sheet, we limit the model domain to a regional catchment area between the Dome Fuji ice divide and the Princess Ragnhild Coast (Fig. 1). Boundary conditions on the model are a fixed ice thickness at the grounding line and a zero surface slope across the ice divide. Grounding-line motion and ice-shelf dynamics were not included, as this study focuses on the inland part of the ice sheet and the ice stream. To create the input files, the BEDMAP data were resampled to a grid of 10 by 10 km, leading to a model domain of 86 by 86 gridpoints in the horizontal, and 41 layers in the vertical.

### Subglacial water and basal sliding

In the model, basal hydrology is represented in terms of the subglacial water flux, which is a function of the basal melt rate. A continuity equation for basal water flow is written as

$$\frac{\partial w}{\partial t} = -\nabla \cdot (\mathbf{v}_w w) + \dot{m}_b, \quad (5)$$

where  $w$  is the thickness of the water layer (m),  $\mathbf{v}_w$  the vertically integrated velocity of water in the layer ( $\text{m a}^{-1}$ ) and  $\dot{m}_b$  the basal melting rate ( $\text{m a}^{-1}$ ). If we consider steady-state conditions, the basal melting rate must balance the water-flux divergence, or  $\dot{m}_b = \nabla \cdot (\mathbf{v}_w w)$ . Basal melting occurs when the ice base reaches the pressure-melting point, and is defined as

$$\dot{m}_b = \frac{1}{\rho_i L} \left( k_i \frac{\partial \theta_b}{\partial z} + G + v_b \tau_b \right), \quad (6)$$

where  $L$  is the latent heat flux,  $G$  is the geothermal heat flux, taken as  $54.6 \text{ mW m}^{-2}$  (Huybrechts, 2002),  $v_b$  is the basal ice velocity,  $\tau_b$  the basal drag and  $\theta_b$  the basal ice temperature. Subglacial water tends to move in the direction of decreasing hydraulic potential  $\phi$  (Shreve, 1972). If we assume that basal water pressure is equal to the overlying ice pressure, the hydraulic potential gradient (or water-pressure gradient) is written as  $\nabla \phi = \rho_i g \nabla z_s + (\rho_w - \rho_i) g \nabla z_b$ , where  $\rho_w$  is the water density and  $z_b$  is the lower surface elevation of the ice mass. The steady-state basal water flux  $\psi_w = (\mathbf{v}_w w)$  is obtained by integrating the basal melt rate  $\dot{m}$  over the whole drainage basin, starting at the hydraulic head in the direction of the hydraulic potential gradient  $\nabla \phi$ . This is done with the computer scheme for balance-flux distribution of ice sheets described in detail by Budd and Warner (1996).

In large-scale ice-sheet modelling, basal sliding is often taken as being proportional to the basal drag (or driving stress) and inversely proportional to the effective pressure, which is defined as the ice overburden pressure minus the basal water pressure. Weertman (1964) relates basal sliding

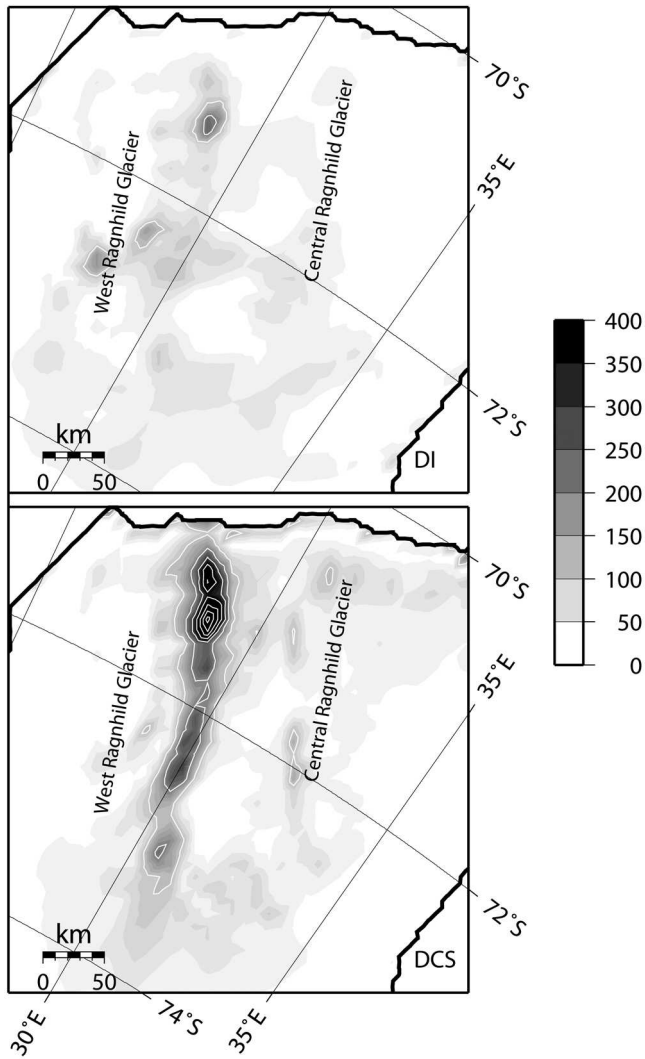


**Fig. 2.** Predicted surface velocity ( $\text{m a}^{-1}$ ) according to the diagnostic isothermal experiment (*DI*) and the thermocoupled experiment with basal sliding (*DCS*).

velocity to the driving stress and a roughness factor. The presence of a thin water film underneath an ice sheet will reduce friction and thus bed roughness, hence facilitating basal sliding. In that sense, it is possible to involve basal water-layer thickness as inversely proportional to roughness (Johnson and Fastook, 2002). However, water-layer thickness can only be determined if the subglacial water velocity is known. For the sake of simplicity, we assume water velocity constant over the whole drainage basin, so that the subglacial water flux  $\psi_w$  can be inversely related to bed roughness. Although we are aware that in some limit cases, such as a subglacial lake where  $\mathbf{v}_w = 0$  but the ice velocity across the lake differs from zero, the above relation breaks down, the model results show that  $\psi_w$  generally increases towards the grounding line. As such, we obtain a sliding law, in its most simple form (linear), written as

$$\mathbf{v}_b = A_b \psi_w \tau_b \exp[-\gamma(\theta_{\text{pmp}} - \theta)], \quad (7)$$

where  $A_b$  is a sliding constant and  $\theta_{\text{pmp}}$  is the pressure-melting temperature. The exponential term in Equation (7) allows for basal sliding at subfreezing temperatures over a range of  $\gamma = 1 \text{ K}$  (Hindmarsh and Le Meur, 2001). Since basal sliding  $\mathbf{v}_b$  also appears in the determination for the

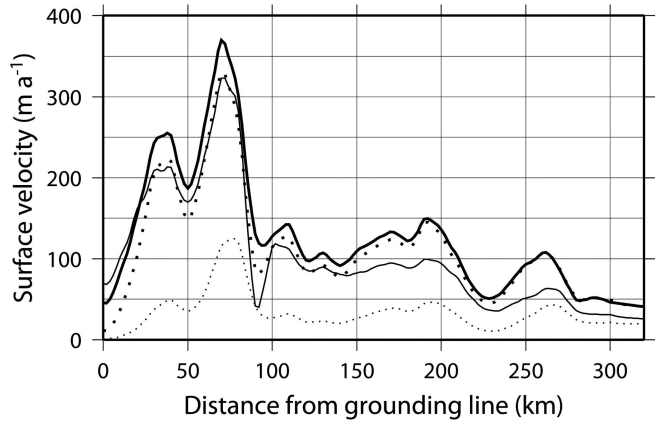


**Fig. 3.** Predicted surface velocity ( $\text{m a}^{-1}$ ) according to the four diagnostic experiments *DI* (small dots), *DC* (large dots), *DIS* (thin line) and *DCS* (thick line).

basal melt rate (Equation (6)), Equation (7) is solved iteratively within each time-step. Basal sliding due to subglacial meltwater is likely to occur in the Ragnhild catchment, as evidence of subglacial water flow is found in deglaciated areas in the coastal part of the adjacent drainage basin (Sawagaki and Hirakawa 1997).

## STANDARD EXPERIMENTS

A first series of experiments are diagnostic in nature, i.e. the velocity, stress and temperature fields were calculated by keeping the glacier geometry (ice thickness) fixed. Four experiments were carried out: an isothermal experiment *DI* where the flow parameter  $A(\theta^*)$  was kept constant at  $2 \times 10^{-17} \text{ Pa}^{-n} \text{ a}^{-1}$ , a model run where the temperature field was coupled to the velocity (*DC*) and two model runs where basal sliding was included (*DIS* and *DCS*). In the thermocoupled experiments (*DC* and *DCS*) the temperature-dependent flow parameter was determined as

$$A(\theta^*) = m a \exp\left(-\frac{Q}{R\theta^*}\right), \quad (8)$$

where  $a = 1.14 \times 10^{-5} \text{ Pa}^{-n} \text{ a}^{-1}$  and  $Q = 60 \text{ kJ mol}^{-1}$  for  $\theta^* < 263.15 \text{ K}$ ,  $a = 5.47 \times 10^{10} \text{ Pa}^{-n} \text{ a}^{-1}$  and  $Q = 139 \text{ kJ mol}^{-1}$  for  $\theta^* \geq 263.15 \text{ K}$ . The enhancement factor was taken as  $m = 2$ , so that modeled and observed velocities are in agreement in experiment *DC*. The sliding rate factor  $A_b$  was set to  $1.3 \times 10^{-3} \text{ Pa}^{-1} \text{ m}$  so that modeled velocities agree with observations in experiment *DIS*. The same parameters were used for experiment *DCS*. For the thermocoupled experiments, the temperature field was each time run to steady state.

Figure 2 displays the predicted velocity according to the *DI* and *DCS* experiments. The isothermal ice-sheet model is not capable of explaining the observed surface velocities nor the pronounced channeling as seen from balance-flux estimates. Introducing thermomechanical coupling and/or basal sliding based on the subglacial water model results in a channeled flow pattern of enhanced ice flow. As seen from Figure 3, sliding and/or coupling result in a similar pattern of ice flow. This striking coincidence becomes clear when comparing the basal water flow with the basal temperature pattern. We therefore calculated the *potential* basal water flow by assuming that the whole ice sheet in the Ragnhild

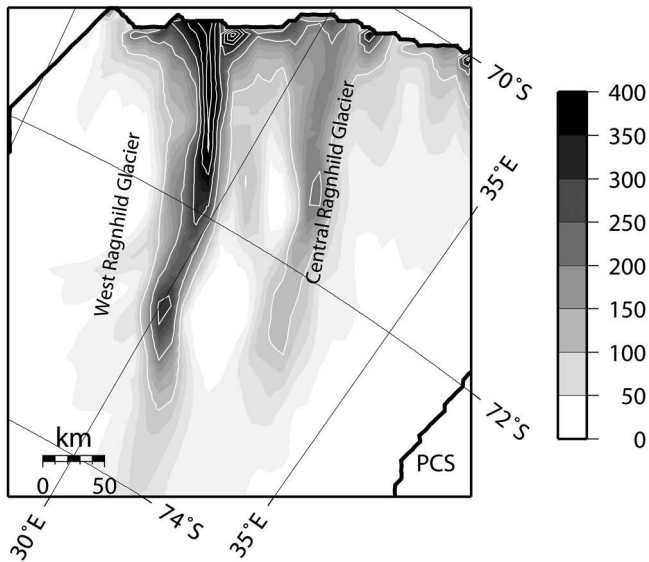


**Fig. 4.** (a) Predicted basal water flux ( $\text{m}^2 \text{a}^{-1}$ ) for a uniform basal melting rate of  $1 \text{ mm a}^{-1}$ . (b) Predicted basal temperature corrected for pressure melting ( $^{\circ}\text{C}$ ) for the *DC* experiment.

drainage basin reached the pressure-melting point at the base, with a constant basal melting rate of  $1 \text{ mm a}^{-1}$ . The result of this exercise is shown in Figure 4a and demonstrates that the basal water flow is concentrated in the topographic lows, hence forming an elongated pattern penetrating far inland for the major ice streams in the area. The basal temperature pattern is quite similar, showing the temperature at pressure-melting point for the same channels (Fig. 4b, experiment *DC*). Introducing basal sliding or temperature coupling leads to a similar pattern in ice flow, with comparable velocities. Cumulating these effects does not alter this pattern nor the magnitude of the surface velocity, although basal sliding is relatively important. The reason for this convergence lies in a negative feedback where increased basal sliding increases the advection of colder ice from above and reduces the amount of vertical shear, hence reducing the thickness of the highly deforming basal ice layer that is at pressure-melting point.

A second series of experiments consists in running the model in prognostic mode, i.e. by allowing the ice thickness to react to the calculated velocity and temperature distribution and running the model to steady state. Four similar experiments were carried out, one isothermal experiment (*PI*), one thermocoupled experiment (*PC*) and two with the addition of basal sliding (*PIS* and *PCS*). Similar to the diagnostic experiments, the pattern of channeled flow is only revealed with basal sliding and/or thermomechanical coupling (Fig. 5). Even more apparent is the signature of CRG in addition to WRG. East Ragnhild glacier remains absent as a discernible feature in the simulation (cf. Fig. 1). The velocity fields from the prognostic experiments are more channelized and reach further inland than the velocity fields from the diagnostic experiments.

### SENSITIVITY OF THE RAGNHILD GLACIERS

The effects of basal sliding on the dynamic behavior of the model are assessed in a series of four experiments in which the value of parameter  $A_b$  in Equation (7) is gradually

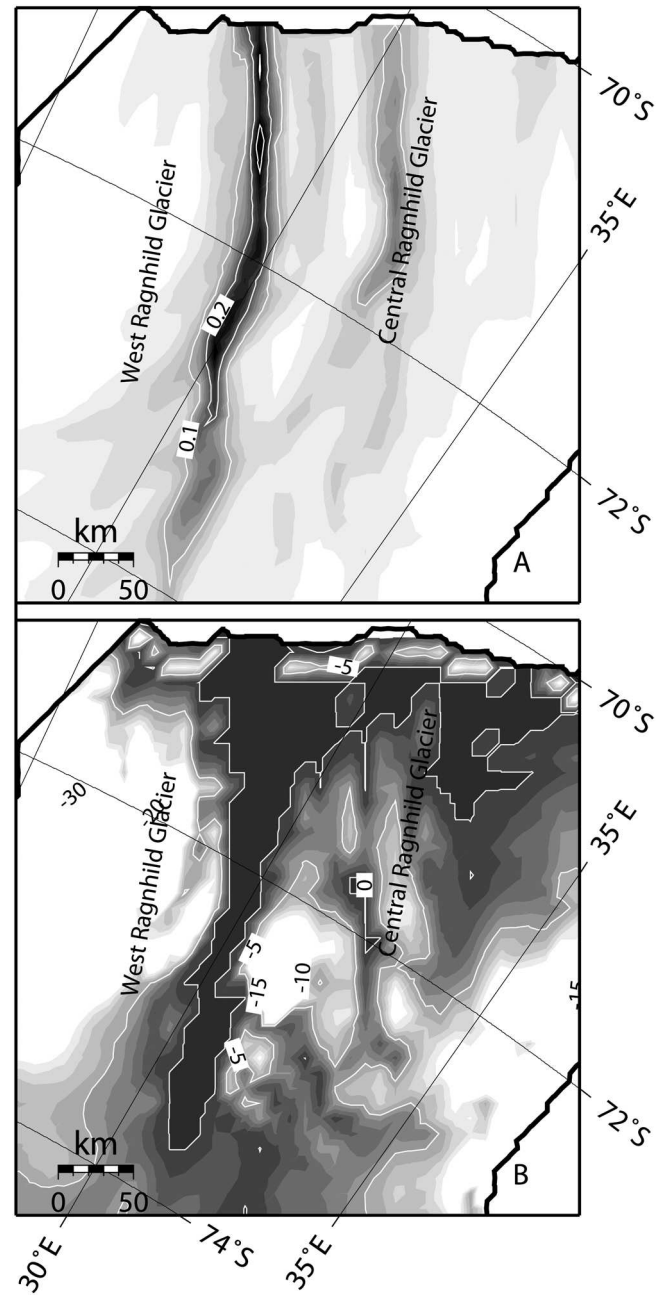


**Fig. 5.** Predicted surface velocity ( $\text{m a}^{-1}$ ) according to the prognostic thermocoupled experiment with basal sliding (*PCS*).

increased, i.e.  $A_b = 1.3, 2.0, 3.3$  and  $5.0 \times 10^{-3} \text{ Pa}^{-1} \text{ m}^{-1}$ . All experiments start from the *PCS* experiment, and are run to a steady state. In each of the experiments a final time-independent solution is achieved. Increasing the basal sliding parameter  $A_b$  leads to an acceleration of WRG and a deceleration of CRG (Fig. 6). The origin of this dynamic behavior lies in ice piracy by WRG (Fig. 7). Increased basal sliding allows WRG to drain more ice from the upper part of the drainage basin. The surface topography lowers within the fast-flowing corridor, so that surface slopes at the edge with the slower-moving ice increase and both ice and basal water are drawn towards this fast-flow corridor, which also narrows to compensate for the high ice flux in the center (Figs 6 and 7). Although CRG could potentially exhibit a similar behavior, the larger WRG grows faster than the smaller CRG. Therefore, the drainage zone of CRG gradually

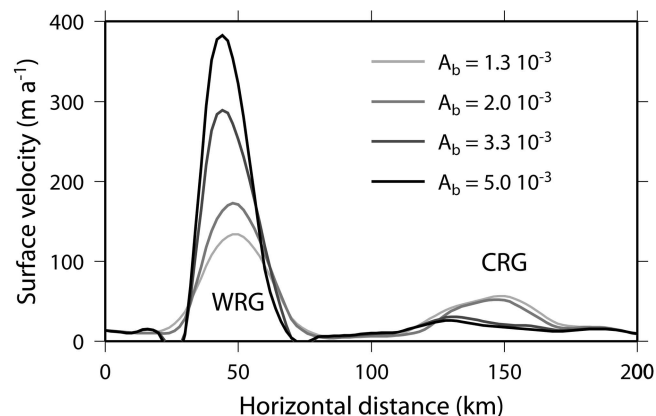


**Fig. 6.** Cross-section through WRG and CRG of predicted surface velocity, according to different basal sliding parameterizations.

decreases in size, decreasing the local ice flux, so that CRG eventually shuts down. Anandakrishnan and Alley (1997) showed that the slow-down of Ice Stream C occurred because of loss of lubrication at the bed, due to a bump in the glacier bed that has directed lubricating water to the neighboring Whillans Ice Stream. For the Ragnhild glaciers, water piracy is more a result of the ice piracy, as the direction of the subglacial water flow, governed by the potential gradient, is largely determined by the surface slope of the ice sheet.

## DISCUSSION

Stokes and Clark (1999) make a distinction between pure and topographic ice streams, because an outlet glacier does not need to be associated with enhanced flow rates. Bentley (1987), however, claims that topographically controlled ice streams or outlet glaciers are associated with enhanced flow velocities as there is a tendency for ice flow to accelerate within topographically constrained corridors. The main reasons for occurrence of enhanced ice flow in topographic ice streams are summed up by Bennett (2003): higher temperatures leading to enhanced ice flow are likely to occur as the ice is thicker, which allows for better isolation. Thicker ice also leads to higher driving stresses, hence higher velocities, which results in increased strain heating. Finally, most of the meltwater will be produced in these topographic lows at pressure-melting point, enhancing basal sliding. However, the whole process does not necessarily need to turn into a feedback system that leads to flow acceleration and (partial) disintegration of the ice sheet (Clarke and others, 1977). The combined effect of basal sliding and ice softening due to thermomechanical coupling results in a relatively stable ice-sheet configuration. Even a prescribed increase in lubrication (through parameter  $A_b$ ) does not lead to a periodic switch between fast and slow ice flow (Payne, 1995; Pattyn, 1996), nor does it lead to a switching behavior between ice streams in a time dependency, as reported by Payne (1998) for the Siple Coast ice streams.

Comparison of Norwegian and Belgian maps with RADARSAT imagery points to a speed-up of the ice in the western part of the Ragnhild Coast and a slow-down to the east. Although the dynamic experiments and balance-flux estimates clearly show the presence of at least two ice

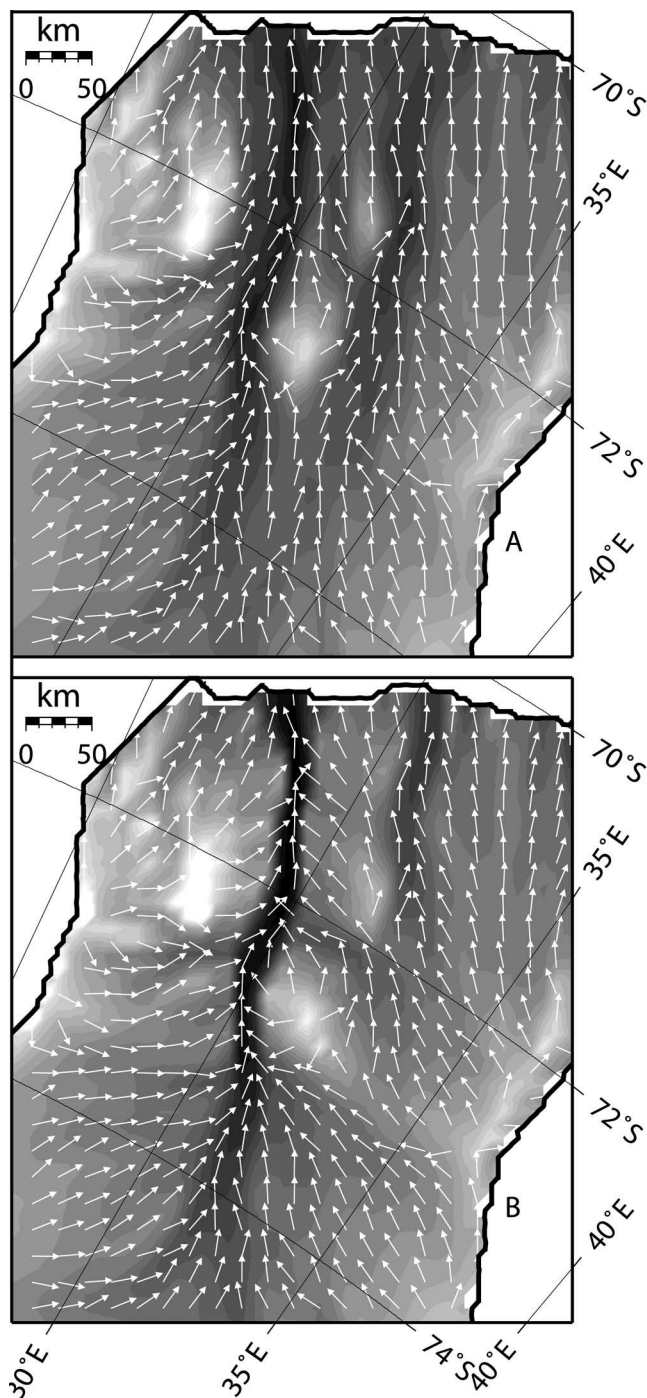


**Fig. 7.** Predicted steady-state ice flux according to the basal sliding experiment with  $A_b = 1.3 \times 10^{-3}$  (a) and  $A_b = 5.0 \times 10^{-3}$  (b). Arrows show the direction of basal water flow.

streams, the diagnostic experiments fail to reproduce CRG or other flow features in the east of the drainage basin. Observed inland ice velocities also show a much higher flow speed for WRG than for the adjacent CRG. Sensitivity experiments demonstrate that a speed-up of WRG causes ice piracy which eventually leads to a stoppage of CRG. In view of the above observations, such a process might already be underway.

One major distinction between an outlet glacier and the enhanced-flow zone of WRG is that the latter is not flanked by surrounding mountains. Rutford Ice Stream, for instance, is at one side flanked by mountains (and hence a real outlet

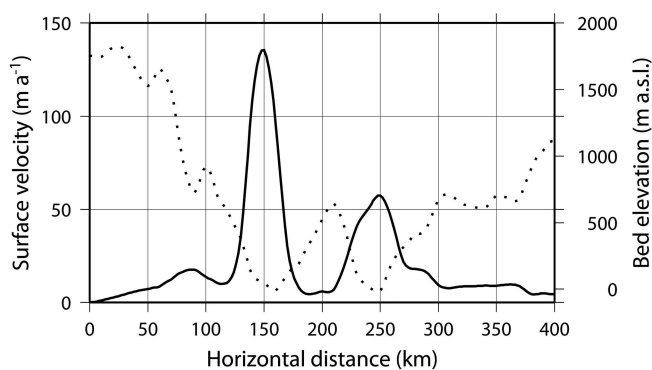


**Fig. 8.** Cross-section through WRG and CRG of predicted surface velocity and bed elevation.

glacier) but flanked by slower-moving ice at the other side (Bentley, 1987). WRG, by contrast, lies in a broad valley, but the fast-moving ice is flanked by surrounding slower-moving ice, and distinct shear margins can be traced all along the glacier within the ice. The fast-flow zone is not wider than 30 km within a valley that is >100 km wide (Fig. 8). The narrowing becomes more pronounced as basal sliding increases (Fig. 7).

## CONCLUSIONS

Ice flow within the East Antarctic ice sheet seems rather complex, and the interior plateau is drained by large elongated features of enhanced ice flow. The Ragnhild glaciers are such features penetrating several hundred kilometers inland. Enhanced ice flow is due to thermo-mechanical effects and the role of basal sliding in topographic lows. Although the position of these glaciers is topographically controlled, these fast-flow zones are not flanked by rock outcrops at the surface. Hence they differ from outlet glaciers by the presence of shear margins *within* the ice sheet penetrating far inland. An increased lubrication of these glaciers results in ice piracy by WRG which leads to a progressive stoppage of CRG, a process that in view of observations might already be underway.

## ACKNOWLEDGEMENTS

This paper forms a contribution to the Belgian Research Programme on the Antarctic (Belgian Science Policy Office), contract EV/03/08 (AMICS). S.D.B. is supported by a PhD grant of the Institute for the Promotion of Innovation by Science and Technology in Flanders (IWT). The authors are indebted to J.S. Walder and G. Flowers for their valuable help in improving the manuscript.

## REFERENCES

Anandakrishnan, S. and R.B. Alley. 1997. Stagnation of Ice Stream C, West Antarctica by water piracy. *Geophys. Res. Lett.*, **24**(3), 265–268.

Bamber, J.L., D.G. Vaughan and I. Joughin. 2000. Widespread complex flow in the interior of the Antarctic ice sheet. *Science*, **287**(5456), 1248–1250.

Bennett, M.R. 2003. Ice streams as the arteries of an ice sheet: their mechanics, stability and significance. *Earth-Science Reviews*, **61**(3–4), 309–339.

Bentley, C.R. 1987. Antarctic ice streams: a review. *J. Geophys. Res.*, **92**(B9), 8843–8858.

Bindschadler, R., J. Bamber and S. Anandakrishnan. 2001. Onset of streaming flow in the Siple Coast region, West Antarctica. In Alley, R.B. and R.A. Bindschadler, eds. *The West Antarctic ice sheet: behavior and environment*. Antarctic Research Series, 77. Washington, DC, American Geophysical Union, 123–136.

Budd, W.F. and R.C. Warner. 1996. A computer scheme for rapid calculations of balance-flux distributions. *Ann. Glaciol.*, **23**, 21–27.

Clarke, G.K.C., U. Nitsan and W.S.B. Paterson. 1977. Strain heating and creep instability in glaciers and ice sheets. *Rev. Geophys. Space Phys.*, **15**(2), 235–247.

Hindmarsh, R.C.A. and E. Le Meur. 2001. Dynamical processes involved in the retreat of marine ice sheets. *J. Glaciol.*, **47**(157), 271–282.

Huybrechts, P. 2002. Sea-level changes at the LGM from ice-dynamic reconstructions of the Greenland and Antarctic ice sheets during the glacial cycles. *Quat. Sci. Rev.*, **21**(1–3), 203–231.

Jezek, K. and RAMP Product Team. 2002. *RAMP AMM-1 SAR image mosaic of Antarctica*. Fairbanks, AK, Alaska SAR Facility, in association with the National Snow and Ice Data Centre, Boulder, CO.

Johnson, J. and J. Fastook. 2002. Northern Hemisphere glaciation and its sensitivity to basal melt water. *Quat. Int.*, **95–6**, 65–74.

Joughin, I. and 7 others. 1999. Tributaries of West Antarctic ice streams revealed by RADARSAT interferometry. *Science*, **286**(5438), 283–286.

Joughin, I., M. Fahnestock, D. MacAyeal, J.L. Bamber and P. Gogineni. 2001. Observation and analysis of ice flow in the largest Greenland ice stream. *J. Geophys. Res.*, **106**(D24), 34,021–34,034.

Liu, H., K.C. Jezek and B. Li. 1999. Development of an Antarctic digital elevation model by integrating cartographic and remotely sensed data: a geographic information system based approach. *J. Geophys. Res.*, **104**(B10), 23,199–23,213.

Lythe, M.B., D.G. Vaughan and BEDMAP consortium. 2001. BEDMAP: a new ice thickness and subglacial topographic model of Antarctica. *J. Geophys. Res.*, **106**(B6), 11,335–11,351.

Nishio, F., M. Ishikawa, H. Ohmae, S. Takahashi and T. Katsushima. 1984. A preliminary study of the area between Breid Bay and the Sør Rondane Mountains in Queen Maud Land, East Antarctica. *Antarct. Rec.*, **83**(3), 11–28.

Nishio, F., S. Uratsuka and K. Ohmae. 1995. Bedrock topography. In Higashi, A., ed. *Antarctica, East Queen Maud Land, Enderby Land: glaciological folio*. Tokyo, National Institute of Polar Research.

Paterson, W.S.B. 1994. *The physics of glaciers. Third edition*. Oxford, etc., Elsevier.

Pattyn, F. 1996. Numerical modelling of a fast-flowing outlet glacier: experiments with different basal conditions. *Ann. Glaciol.*, **23**, 237–246.

Pattyn, F. 2003. A new 3D highest-order thermodynamical ice-sheet model: basic sensitivity, ice-stream development and ice flow across subglacial lakes. *J. Geophys. Res.*, **108**(B8), 2382.

Pattyn, F. and R. Naruse. 2003. The nature of complex ice flow in Shirase Glacier catchment, East Antarctica. *J. Glaciol.*, **49**(166), 429–436.

Payne, A.J. 1995. Limit cycles in the basal thermal regime of ice sheets. *J. Geophys. Res.*, **100**(B3), 4249–4263.

Payne, A.J. 1998. Dynamics of the Siple Coast ice streams, West Antarctica: results from a thermomechanical ice sheet model. *Geophys. Res. Lett.*, **25**(16), 3173–3176.

Rippin, D.M., J.L. Bamber, M.J. Siegert, D.G. Vaughan and H.F.J. Corr. 2003. Basal topography and ice flow in the Bailey/Slessor region of East Antarctica. *J. Geophys. Res.*, **108**(F1), 6008.

- Sawagaki, T. and K. Hirakawa. 1997. Erosion of bedrock by subglacial meltwater, Soya Coast, East Antarctica. *Geogr. Ann.*, **79A**(4), 223–238.
- Shreve, R.L. 1972. Movement of water in glaciers. *J. Glaciol.*, **11**(62), 205–214.
- Stokes, C.R. and C.D. Clark. 1999. Geomorphological criteria for identifying Pleistocene ice streams. *Ann. Glaciol.*, **28**, 67–74.
- Takahashi, S., R. Naruse, F. Nishio and O. Watanabe. 2003. Features of ice sheet flow in East Dronning Maud Land, East Antarctica. *Polar Meteorol. Glaciol.*, **17**, 1–14.
- Testut, L., R. Hurd, R. Coleman, F. Rémy and B. Legrésy. 2003. Comparison between computed balance velocities and GPS measurements in the Lambert Glacier basin, East Antarctica. *Ann. Glaciol.*, **37**, 337–344.
- Vaughan, D.G., J.L. Bamber, M.B. Giovinetto, J. Russell and A.P.R. Cooper. 1999. Reassessment of net surface mass balance in Antarctica. *J. Climate*, **12**(4), 933–946.
- Weertman, J. 1964. The theory of glacier sliding. *J. Glaciol.*, **5**(39), 287–303.